A Fictitious Domain Method for Conformal Modeling of the Perfect Electric Conductors in the FDTD Method

Francis Collino, Sylvain Garcés, and Patrick Joly

***Abstract*—We present a fictitious domain method to avoid the staircase approximation in the study of perfect electric conductors (PEC) in the finite-difference time-domain (FDTD) method. The idea is to extend the electromagnetic field inside the PEC and to introduce a new unknown, the surface electric current density to ensure the vanishing of the tangential components of the electric field on the boundary of the PEC. This requires the use of two independent meshes: a regular three-dimensional (3-D) cubic lattice for the electromagnetic field and a triangular surface-patching for the surface electric current density. The intersection of these two meshes gives a simple coupling law between the electric field and the surface electric current density. An interesting property of this method is that it provides the surface electric current density at each time step. Furthermore, this method looks like FDTD with a special model for the PEC. Numerical results for several objects are presented.**

***Index Terms*— FDTD methods, fictitious domain, Maxwell's equations, time-domain methods.**

I. Introduction

THE finite-difference time-domain (FDTD) method is a well-known powerful numerical technique for solving the Maxwell's time-dependent curl equations [1]. The main drawback of this method is the staircase meshing. The structures are described with a uniform rectangular lattice so when the staircase approximation for curved interfaces is used, numerical scattering can appear and disturb the computed solution [2].

Several solutions to this problem have been proposed. A quasi-nonuniform grid FDTD algorithm was proposed that is well suited for the study of planar microwave circuits [3]. In order to try to match curved interfaces, some methods the use of irregular nonorthogonal structured grids is proposed elsewhere [4]. In other solutions the uniform rectangular lattice is retained and Yee algorithm is locally modified to take into account curved interfaces. According to this idea, perfect electric conductor (PEC) structures are modeled by contour-path approach in two-dimensional (2-D) case [5] and three-dimensional (3-D) case [6]. This method of contour path FDTD (CPFDTD) is certainly the most popular one for the treatment of complex PEC and has been studied by many research groups, e.g., [7]–[9]. Its main advantage is that it keeps the structure of Yee's algorithm and can thus use the classical techniques developed for FDTD, such as absorbing boundary conditions or post processing. However, the stability criterion depends on the geometry of the metallic scatterers and can be difficult to control.

In this paper, we present a fictitious domain method, for analysis of 3-D electromagnetic scattering by a PEC. Fictitious domain methods have been introduced to solve stationary problems [10]–[12], and have been proposed recently for the Maxwell scattering problem in the 2-D case [13], [14]. The extension to the 3-D case that is presented here was originally developed in [15].

Manuscript received June 11, 1997; revised January 12, 1998. This work was supported by the Centre National d'Etudes des Télécommunication at La Turbie, France.

F. Collino is with the Centre Européen de Recherche et de Formation, Appliquées au Calcul Scientifique, Toulouse, France.

S. Garcés is with the Centre National d'Etudes des Télécommunications, La Turbie, France.

P. Joly is with Institut National de Recherches en Informatique et Automatique, Rocquencourt, France.

Publisher Item Identifier S 0018-926X(98)07500-0.

II. Fictitious Domain Method

A. Variational Principles

Let $\Omega = \Omega^i$ be a bounded domain in $\mathbb{R}^3$ with boundary $\Gamma = \partial\Omega$, unit outward normal n and $\Omega^e = {}^c\overline{\Omega}$ the exterior of the PEC. The main idea of the fictitious domain method is to extend the electromagnetic field (E, H) to the inside of the PEC Ω and to solve Maxwell's equations inside and outside the PEC. Multiplying Ampere's law by any electric field ϕ defined in $\mathbb{R}^3$ (vacuum and the interior of the PEC) and integrating the curl term by parts, we obtain for the interior problem

$$\varepsilon_0 \int_{\Omega^i} \frac{\partial E}{\partial t} \cdot \phi \, dx - \int_{\Omega^i} H \cdot \nabla \times \phi - \int_{\Gamma} (H \times n)^i \cdot ((\phi \times n) \times n) \, d\gamma = 0. \tag{1}$$

Similarly, for the exterior problem we have

$$\varepsilon_0 \int_{\Omega^e} \frac{\partial E}{\partial t} \cdot \phi \, dx - \int_{\Omega^e} H \cdot \nabla \times \phi \, dx + \int_{\Gamma} (H \times n)^e \cdot ((\phi \times n) \times n) \, d\gamma = 0. \tag{2}$$

We add these two equations in order to obtain the fictitious domain formulation of Ampere's law

$$\varepsilon_0 \int_{\mathbb{R}^3} \frac{\partial E}{\partial t} \cdot \phi \, dx - \int_{\mathbb{R}^3} H \cdot (\nabla \times \phi) \, dx + \int_{\Gamma} j_s \cdot ((\phi \times n) \times n) \, d\gamma = 0 \tag{3}$$

0018–926X/98$10.00 © 1998 IEEE

where $j_s = (H \times n)^e|_\Gamma - (H \times n)^i|_\Gamma$ is the surface electric current density.

We then multiply Faraday's law by any magnetic field ψ defined in $\mathbb{R}^3$ (vacuum and the interior of the PEC), and we obtain the following:

$$\mu_0 \int_{\mathbb{R}^3} \frac{\partial H}{\partial t} \cdot \psi + \int_{\mathbb{R}^3} \psi \cdot (\nabla \times E) = 0. \tag{4}$$

We add a third equation to take into account the vanishing of the tangential components of the electric field on the boundary of the PEC. For any surface electric current density ξ defined on the boundary of the PEC, we have

$$\int_\Gamma ((E \times n) \times n) \cdot \xi \, d\gamma = 0. \tag{5}$$

Gathering (3)–(5), we obtain the mathematical formulation of the fictitious domain method: find the electric field E in the functional space $H(\text{curl}, \mathbb{R}^3)$, the magnetic field H in $H(\text{div}, \mathbb{R}^3)$ and the surface electric current density j_s in $H^{-(1/2)}(\text{div}, \Gamma)$ such that with $(.,.)$ the inner product in $(L^2(\mathbb{R}^3))^3$

$$\forall \phi \in H(\text{curl}, \mathbb{R}^3), \left(\varepsilon_0 \frac{\partial E}{\partial t}, \phi\right) - (H, \nabla \times \phi) + \int_\Gamma ((\phi \times n) \times n) \cdot j_s \, d\gamma = 0 \tag{6}$$

$$\forall \psi \in H(\text{div}, \mathbb{R}^3), \left(\mu_0 \frac{\partial H}{\partial t}, \psi\right) + (\psi, \nabla \times E) = 0 \tag{7}$$

$$\forall \xi \in H^{-(1/2)}(\text{div}, \Gamma), \int_\Gamma ((E \times n) \times n) \cdot \xi \, d\gamma = 0 \tag{8}$$

subject to initial conditions

$$E(t=0) = E_0 \quad \text{and} \quad H(t=0) = H_0. \tag{9}$$

The functional spaces $H(\text{curl}, \mathbb{R}^3)$ and $H(\text{div}, \mathbb{R}^3)$ are the spaces of square integrable functions defined in $\mathbb{R}^3$ whose curl and divergence, respectively, are also square integrable functions. An important property of these spaces is that the tangential, respectively, normal, components of a function of $H(\text{curl}, \mathbb{R}^3)$, respectively $H(\text{div}, \mathbb{R}^3)$, are continuous across interfaces. The space $H^{-1/2}(\text{div}, \Gamma)$ is the natural functional space of the surface electric current densities. They are vector fields tangent to the boundary Γ with some appropriate regularity (see [16] for a complete discussion of these functional spaces).

In [15], we proved that this problem has an unique solution. Furthermore, if (E, H, j_s) is the solution of the fictitious domain problem, then the restriction of the electromagnetic field (E, H) to the exterior Ω^e is the solution of the original problem of the scattering by a PEC.

B. Derivation of the Fictitious Domain Scheme

1) Finite Element Spaces: We introduce two independent meshes. First, the cubic domain including the vacuum and the interior of the PEC is divided into identical small cubes.

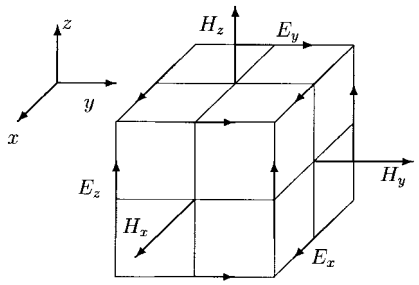

Fig. 1. Position of the degrees of freedom for the electric and magnetic field about a cubic cell of the 3-D space lattice.

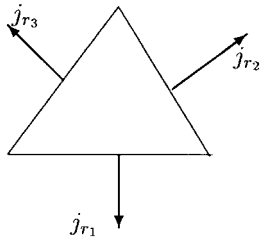

Fig. 2. Position of the degrees of freedom for the surface electric current density about a triangular surface patch of the interface vacuum PEC.

The electric field E is then approximated by the lowest order Nédelec elements for $H(\text{curl})$ and the magnetic field H is approximated by the lowest order Nédelec elements for $H(\text{div})$ [17].

Second, the boundary of the PEC is divided into triangular surface patches and the surface electric current density j_s is approximated by the lowest order Raviart–Thomas element for $H(\text{div}, \Gamma)$ [18]. Note that we have used for the surface electric current density j_s the same finite elements than those of the electric field integral equation (EFIE) method.

Let Δt be the time increment. We compute the electric field E at time step n, and both the magnetic field H and the surface electric current density j_s at time step $n+1/2$. Thus, we have for a point $x \in \mathbb{R}^3$ and a point $x_s \in \Gamma$

$$E(n\Delta t, x) = \sum_{p=1}^{N_{edge}} E_p^n v_p(x) \tag{10}$$

$$H\left((n+\tfrac{1}{2})\Delta t, x\right) = \sum_{q=1}^{N_{face}} H_q^{n+(1/2)} w_q(x) \tag{11}$$

$$j_s\left((n+\tfrac{1}{2})\Delta t, x_s\right) = \sum_{r=1}^{n_{edge}} j_r^{n+(1/2)} \chi_r(x_s) \tag{12}$$

with v_p, w_q, and χ_r appropriate basis functions, N_{edge} and N_{face} the number of edges and faces in the uniform 3-D mesh and n_{edge} the number of edges in the surface mesh. The degrees of freedom of the electric and magnetic fields are, respectively, the tangential components on the edges and the normal components on the faces of the cubes of the 3-D mesh (see Fig. 1) and the degrees of freedom of the surface electric current density are the fluxes across the edges of the triangles of the conformal triangulation (see Fig. 2).

2) Numerical Scheme: Let

$$\begin{cases} \mathcal{E}^n = (E_p^n)_{1\le p\le N_{\text{edge}}} \\ \mathcal{H}^{n+(1/2)} = (H_q^{n+(1/2)})_{1\le q\le N_{\text{face}}} \\ \text{and } \mathcal{J}_s^{n+(1/2)} = (j_r^{n+(1/2)})_{1\le r\le n_{\text{edge}}}. \end{cases} \tag{13}$$

Using central-difference approximation, we obtain the following numerical scheme:

$$M_e\frac{\mathcal{E}^{n+1}-\mathcal{E}^n}{\Delta t} - A\mathcal{H}^{n+(1/2)} + B^T\mathcal{J}_s^{n+(1/2)} = 0 \tag{14}$$

$$M_h\frac{\mathcal{H}^{n+(1/2)}-\mathcal{H}^{n-(1/2)}}{\Delta t} + A^T\mathcal{E}^n = 0 \tag{15}$$

$$B\mathcal{E}^n = 0 \tag{16}$$

with

$$\begin{aligned} [M_e]_{(p,p')} &= \varepsilon_0\,(v_p,\, v_{p'}) \text{ the electric mass matrix} \\ [M_h]_{(q,q')} &= \mu_0\,(w_q,\, w_{q'}) \text{ the magnetic mass matrix} \\ [A]_{(p,q)} &= (\nabla\times v_p,\, w_q) \text{ the stiffness matrix} \\ [B]_{(p,r)} &= \int_\Gamma ((v_p\times n)\times n)\cdot\chi_r d\gamma \text{ the coupling matrix.} \end{aligned}$$

Let h be the space increment in the uniform mesh. Because we choose identical cubes for the 3-D mesh, we apply mass lumping to diagonalize the mass matrices

$$M_e \simeq \varepsilon_0 h^3\, I_d \quad \text{and} \quad M_h \simeq \mu_0 h^3 I_d. \tag{17}$$

We use the same technique to compute the stiffness matrix A. Then the numerical scheme is nothing but like the Yee's scheme [1] where we add the electric field

$$\mathcal{E}^{r,\,n+(1/2)} = \frac{\Delta t}{\varepsilon_0}B^T\mathcal{J}_s^{n+(1/2)} \tag{18}$$

radiated by the surface electric current $\mathcal{J}_s^{n+(1/2)}$ density. In other words, following the Yee's notation, we have for the x component of the electric field

$$\begin{aligned} E_x|_{i,j,k}^{n+1} = {} & E_x|_{i,j,k}^{n} + E_x^{r,\,n+(1/2)}|_{i,j,k} \\ & + \frac{\Delta t}{\varepsilon_0 h}\left(H_z\Big|_{i,\,j+(1/2),\,k}^{n+(1/2)} - H_z\Big|_{i,\,j-(1/2),\,k}^{n+(1/2)}\right) \\ & - \frac{\Delta t}{\varepsilon_0 h}\left(H_y\Big|_{i,\,j,\,k+(1/2)}^{n+(1/2)} - H_y\Big|_{i,\,j,\,k-(1/2)}^{n+(1/2)}\right). \end{aligned} \tag{19}$$

Multiplying by the coupling matrix B in (14) and writing (16) for time steps n and $n+1$, we find that the surface electric current density $\mathcal{J}_s^{n+(1/2)}$ satisfies the linear system

$$(BB^T)\mathcal{J}_s^{n+(1/2)} = BA\mathcal{H}^{n+(1/2)}. \tag{20}$$

Knowing the magnetic field $\mathcal{H}^{n-(1/2)}$ at time step $n-(1/2)$ and the electric field $\mathcal{E}^n$ at time step n, we compute first the magnetic field $\mathcal{H}^{n+(1/2)}$ with (15). Then we solve the linear system (20) to obtain the surface electric current density $\mathcal{J}_s^{n+(1/2)}$ at time step $n+(1/2)$. Finally, we find the electric field $\mathcal{E}^{n+1}$ at time step $n+1$ using (14).

In practice, we prefer the following equivalent algorithm. The computation of the magnetic field $\mathcal{H}^{n+(1/2)}$ is unchanged. In the same manner we compute the electric field $\mathcal{E}_{yee}^{n+1}$ with

$$M_e\frac{\mathcal{E}_{yee}^{n+1}-\mathcal{E}^n}{\Delta t} - A\mathcal{H}^{n+(1/2)} = 0. \tag{21}$$

This step is identical to Ampere's law in Yee's scheme, but we apply it ignoring the PEC. At this stage the tangential components of the electric field $\mathcal{E}_{yee}^{n+1}$ on the boundary of the PEC are not equal to zero. Then we solve the linear system

$$(BB^T)\mathcal{J}_s^{n+(1/2)} = \frac{\varepsilon_0}{\Delta t}B\mathcal{E}_{yee}^{n+1} \tag{22}$$

to obtain the surface electric current density $\mathcal{J}_s^{n+(1/2)}$. Finally, we compute the electric field $\mathcal{E}^{n+1}$ at time step $n+1$ with

$$\mathcal{E}^{n+1} = \mathcal{E}_{yee}^{n+1} - \frac{\Delta t}{\varepsilon_0}B^T\mathcal{J}_s^{n+(1/2)}. \tag{23}$$

So the surface electric current density $\mathcal{J}_s^{n+(1/2)}$ radiates an electric field which forces the tangential components of the electric field $\mathcal{E}^{n+1}$ on the boundary of the scatterer to be equal to zero in a weak sense.

With energy techniques, we proved [15] that for any triangular surface mesh, this numerical scheme is stable as long as the time step Δt and the space increment h of the uniform cubic 3-D lattice satisfy the usual condition

$$\Delta t \le \frac{h}{c_0\sqrt{3}} \quad \text{where} \quad c_0 = \frac{1}{\sqrt{\varepsilon_0\mu_0}}. \tag{24}$$

This property is true for both open problems (or scattering problems) and closed problems (or resonators). This very simple stability criterion outlines the main difference between our scheme and other time-domain methods which use conformal meshes [4]. For such methods, the stability criterion has to be found for each mesh [19], a procedure that is often computationally expensive.

3) The Electric Coupling Matrix: The matrix B couples the electric field and the surface current density. It is a rectangular real matrix with coefficients

$$b_{p,r} = \int_\Gamma ((v_p\times n)\times n)\cdot\chi_r\, d\gamma. \tag{25}$$

The support of the basis element v_p is the union off our adjacent cubes and the support of the basis element χ_r is the union of two adjacent triangles (see Fig. 3). In general, the computation of the coefficients $b_{p,r}$ requires to compute the intersection of cubes and triangles. We proved that the intersection of a cube and a triangle is a convex polygon with less than nine edges and we proposed an efficient algorithm to compute this intersection (see [15] for the complete description of this numerical aspect). Moreover, the coefficient $b_{p,r}$ is equal to zero if the supports of the two basis functions v_p and χ_r are disjoint. For example, in Fig. 3 the electric basis function v_p is coupled with the electric current basis function χ_r because the intersection of their supports is not empty

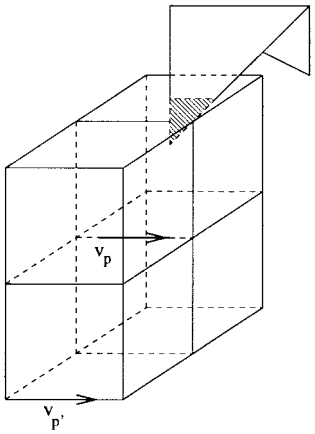

Fig. 3. Intersection of cubes and triangles for the computation of the electric coupling matrix B.

(dashed polygon). On the contrary, $v_{p'}$ and χ_r are not coupled. So the coupling matrix B is a very sparse matrix.

The matrix BB^T is then a real positive symmetric sparse matrix, however, we have not yet established that it is positive definite. Let h_{2D} denote the shortest length of the edge of the triangular patches of the interfaces between the vacuum and the PEC. We found that if $h_{2D} \ll h$, then the matrix BB^T is singular. We can explain this physically. At each step time, we compute the surface electric current density, but we take into account the wave propagation via Yee's algorithm instead of with the delayed potentials. So when $h_{2D} \ll h$, the wave cannot propagate well.

Conversely, we proved that when $h > h_{2D}$, for the 2-D TE case the matrix BB^T is not singular [15]. In practice, for the 3-D case numerical results show that the matrix BB^T is a positive definite matrix as soon as $h > h_{2D}$. This result agrees with previous results for the homogeneous elliptic Dirichlet problem [20].

The square matrix BB^T has dimension n_{edge}^2, where n_{edge} is the number of degrees of freedom for the surface electric current density. For industrial cases n_{edge} is about 10 000. This number is much smaller than the number of degrees of freedom for the electric and magnetic fields, which can reach 1 000 000.

Finally, we recall that the coupling matrix is independent of the time step, and depends only on the geometry of the scattering problem.

III. Numerical Results

A FDTD code with Bérenger perfectly matched layer (PML), [21] is used for simulations. Subroutines to treat PEC with the fictitious domain method are added to this code. Before the main FDTD time stepping loop, the coupling matrix B and the square matrix BB^T are computed. Then the Cholesky factorization of matrix BB^T is computed. During the time stepping loop, at each time step the linear system (22) is solved and the radiated electric field (23) is added to the electric field. Finally, after a discrete Fourier transformation, the far-field pattern is obtained.

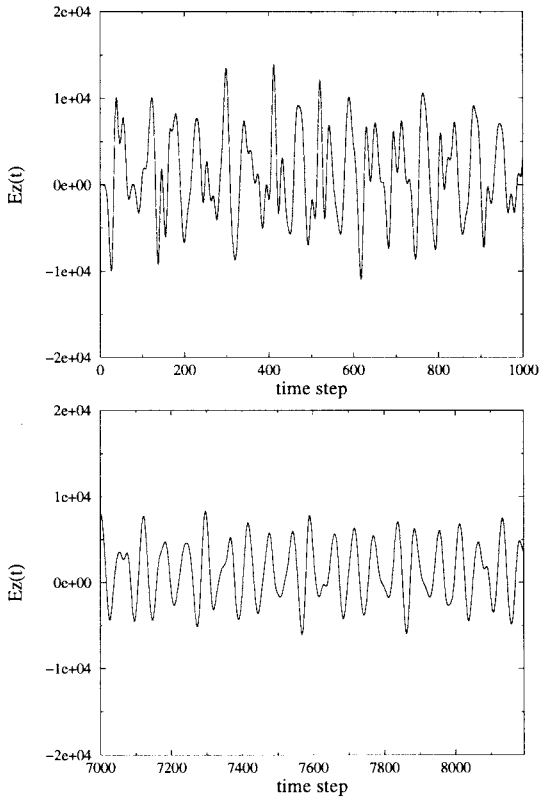

Fig. 4. Electric field $Ez(t)$ at point x, $y = 54$ mm, $z = 55$ mm.

A. Spherical Cavity

The first example is a spherical resonator with radius $a = 15$ mm. In this case, the fictitious domain is now the exterior of the obstacle. This example is an excellent test to confirm experimentally the stability of the numerical scheme that we have obtained theoretically by energy estimates, [14], [15]. The 3-D grid resolution is $h = 1$ mm and the 3-D test grid has 50 $\times$ 50 $\times$ 51 cells. The time increment is $\Delta t = 1.9 \times 10^{-12}$ s, and the run has eight 192 time steps. The boundary of the spherical cavity is meshed with one 144 triangles and one 716 edges whose lengths h' are longer than 1.6 mm and shorter than 3.2 mm. A Gaussian source is excited on a z-directed electric dipole [22] located in the cavity at point $x = 2$ mm, $y = 2$ mm, $z = 2$ mm. In other words, we have

$$\begin{aligned} E_z|_{i_0,\,j_0,\,k_0+(1/2)}^{n+1} &= E_z|_{i_0,\,j_0,\,k_0+(1/2)}^{n+1} + \frac{\Delta t}{\epsilon_0 h}\Big(H_y\Big|_{i_0+(1/2),\,j_0,\,k_0+(1/2)}^{n+(1/2)} \\ &\quad - H_y|_{i_0-(1/2),\,j_0,\,k_0+(1/2)}^{n+(1/2)}\Big) \\ &\quad - \frac{\Delta t}{\epsilon_0 h}\Big(H_x|_{i_0,\,j_0+(1/2),\,k_0+(1/2)}^{n+(1/2)} \\ &\quad - H_x|_{i_0,\,j_0-(1/2),\,k_0+(1/2)}^{n+(1/2)}\Big) + \frac{1}{1000}e^{-a^2(n-n_0)^2} \end{aligned} \tag{26}$$

with $a = 0.014$ and $n_0 = 26$. In practice, this source is active up to time step $n = 2n_0 = 52$. Fig. 4 shows the z component of the electric field recorded at a point A inside

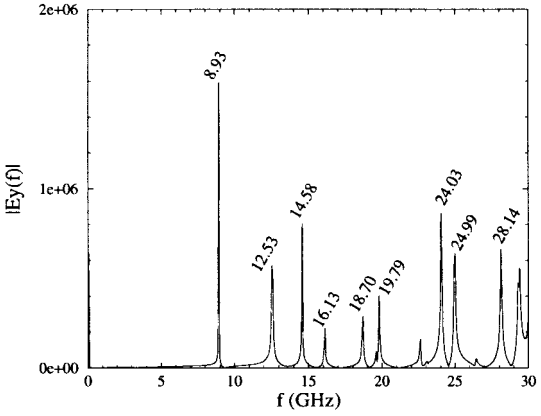

Fig. 5. Electric field $|Ez(f)|$ at point x, $y = 54$ mm, $z = 55$ mm.

the cavity, respectively, at the beginning and at the end of the simulation. The electromagnetic energy is trapped inside the spherical cavity and the electric field oscillates throughout the simulation. Note that there is no numerical instability; the electric field does not diverge.

Fig. 5 shows the discrete Fourier transform of the z component of the electric field at point A. The curve presents picks at frequencies 8.93 GHz, 12.53 GHz, and so on. These values fit with the analytical resonant frequencies of the spherical cavity of radius 15 mm.

B. Scattering by Two Conducting Spheres

The second example is a system of two $k_0a = \pi$ spheres whose centers are separated by two wavelengths. This example was treated by the contour path FDTD method in [5] and is thus a good point for comparison. With this example, our goal is also to show that the fictitious domain method is a good technique to compute radar cross section (RCS) of single and multiple bodies.

The 3-D cell resolution is $\lambda_0/20$ and the test grid is 80 $\times$ 80 $\times$ 80 cells, so there are 3 129 840° of freedom for the electromagnetic field (E, H). The two boundaries of the spheres are discretized with 912 triangles and 1368 edges of length between $\lambda_0/10$ and $\lambda_0/5$. We point out that the number of degrees of freedom for the surface electric current density (1368) is much smaller than the number of degrees of freedom for the electromagnetic field (3 129 840).

Fig. 6 shows the sparsity pattern of the matrix BB^T used for the computation of the surface electric current density. Note that only 2.80% of its coefficients are not zero, and that BB^T is a skyline matrix, with two independent blocks that correspond to the two spheres.

Fig. 7 shows the E-plane bistatic RCS of two spheres. The direction of the propagation of the incident plane wave is 45° off the axis defined by the two spheres' centers. The angle $\Phi = 0$ is the forward scatter direction. Like [5], the fictitious domain method agrees very well with the method of reference. A more precise comparison shows that the fictitious domain method seems to give a slightly more accurate result for the forward scatter direction while it gives slightly less precise results for some other directions.

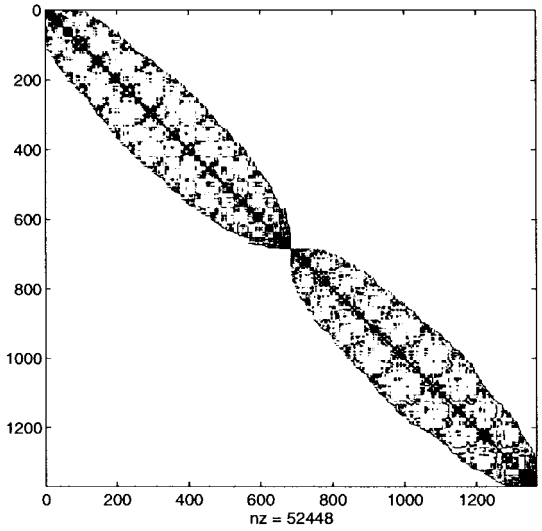

Fig. 6. Sparsity pattern of the matrix BB^T used to compute the surface electric current density; 2.80% of the coefficients are not identically zero.

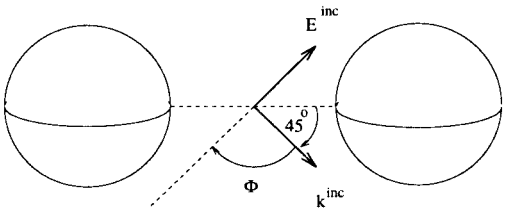

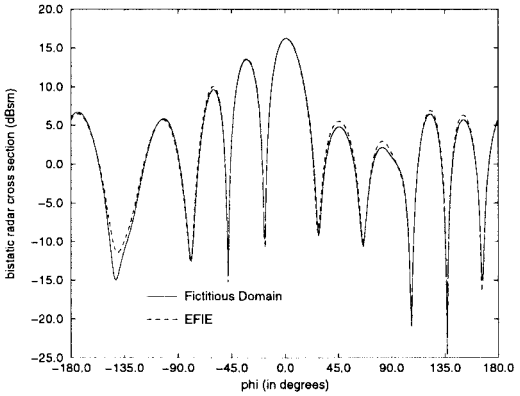

Fig. 7. E-plane bistatic RCS of two $k_0a = \pi$ spheres separated by $2\lambda_0$ air gap.

C. The Radar Cross Section of an Ogive

The next example shows the efficiency of the fictitious domain method for modeling scattering of waves on sharp metallic bodies. We compare the fictitious domain method with the usual FDTD method using staircasing in terms of numerical accuracy and central processing unit (CPU) running time. The PEC is an ogive with nose angle $\theta = 40°$ and diameter $D = 164$ mm (see Fig. 8). The backward RCS of this ogive is compared with calculated data from [23]. The 3-D resolution is $h = 10$ mm, so the diameter D of the ogive is equal to 16.4 cells. The lengths of the 504 edges of the triangular patches are included between 11 and

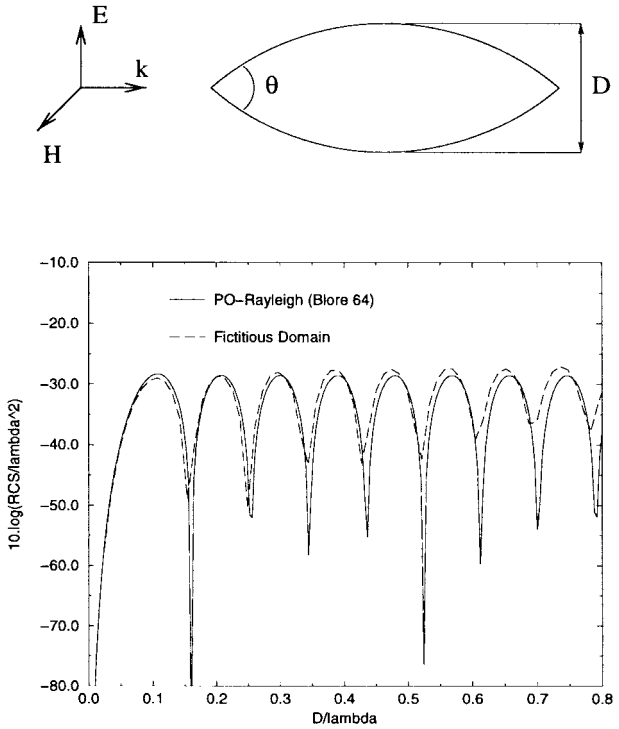

Fig. 8. The backward scattering by a PEC ogive with $\theta = 40^\circ$ $D = 164$ mm. Illumination with a Gaussian pulse.

81 mm. The illumination is a Gaussian pulse such that the excited frequencies of the incident plane wave are inferior to 1.5 GHz. We obtain good agreement between numerical results computed by the fictitious domain method and calculated data (see Fig. 8).

Then we compare the RCS computed with the fictitious domain method and the FDTD method. An EFIE code with a very thin surface mesh for the ogive (6264 edges whose lengths are included between 0.9 and 25 mm) gives the reference. The characteristics of the fictitious domain method are not changed, so the 3-D grid is $120 \times 47 \times 46$ cells with a resolution $h = 10$ mm, 500 time steps with a time resolution $\Delta t = 1.9 \times 10^{-10}$ s, and a conformal mesh with 336 triangles and 504 edges.

For the first FDTD study, we maintained the same space and time resolution with a $120 \times 47 \times 46$ cell 3-D grid and 500 time steps. For the second FDTD study, the space resolution is $h = 5$ mm with $240 \times 93 \times 92$ cells, and the time resolution is $\Delta t = 0.95 \times 10^{-10}$ s with 1000 time steps.

Fig. 9 shows the RCS in the plane orthogonal to the incident magnetic field for frequency $f = 0.96$ GHz. The calculated data are obtained by a normal FDTD near-to-far field transformation [19], for the two FDTD runs, and by a near-to-far field transformation from the surface current density discrete Fourier transform. We find good agreement between the fictitious domain method and the reference. As expected, numerical results are better for FDTD run with resolution $h = 5$ mm $= \lambda_0/66$ than for resolution $h = 10$ mm $= \lambda_0/33$, but even for the greater resolution, FDTD does not give good results in forward and backward directions. The results obtained with the fictitious domain method with

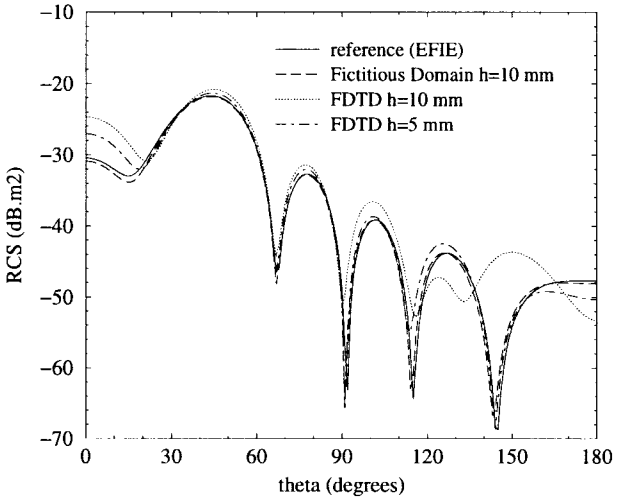

Fig. 9. RCS of a PEC ogive in the plane (k, E), for the frequency $f_0 = 0.96$ GHz, $\lambda_0 = 2.03D$.

TABLE I
SUMMARY OF THE CHARACTERISTICS TO COMPUTE THE RCS OF AN OGIVE

	Fictitious Domain	FDTD	FDTD
h	10 mm	10 mm	5 mm
cells	120 × 47 ×46	120 × 47 ×46	120 × 47 ×92
Δt	1.9 10^{-10} s	1.9 10^{-10} s	0.95 10^{-10} s
$N_{\Delta t}$	500	500	1000
CPU time	11 min	7 min	78 min

resolution $h = 10$ mm are more accurate than those with the usual FDTD method with 5-mm resolution. Table I shows the CPU times for the three tests. The FDTD method with the lower resolution $h = 10$ mm is the fastest with 7 min and the FDTD method with the higher resolution $h = 5$ mm is the slowest at 78 min. CPU time for the fictitious domain method is intermediary at 11 min. The overall cost with respect to FDTD with same h is as follows:

- the assembly of matrix B (6 s);
- the computation of BB^T (18 s);
- the factorization of the matrix BB^T (0.1 s) with an efficient FORTRAN library for sparse matrices;
- at each time step, the computation of the surface current density with (20).

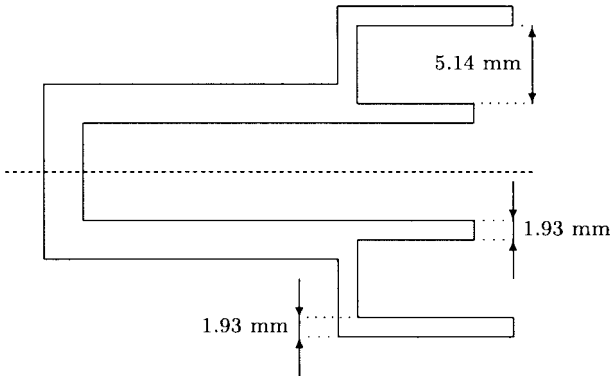

Fig. 10. Geometry of the axisymmetric horn antenna. The diameter of the circular waveguide is 25.7 mm.

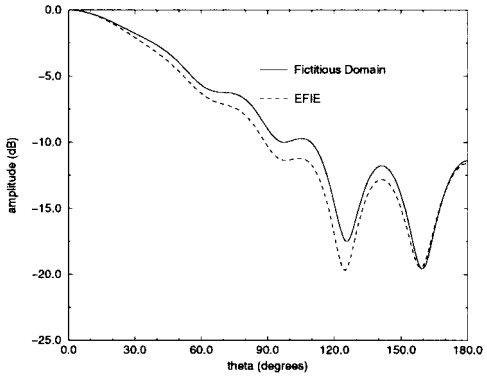

Fig. 11. Radiation pattern of the horn antenna in the E-plane, frequency $F = 7.5$ GHz. Comparison of the fictitious domain method and EFIE.

D. An Axisymmetric Horn Antenna

The radiation of a simple axisymmetric horn antenna is the last example. Fig. 10 presents the geometry of the horn antenna, which is a body of revolution. The circular waveguide has a diameter equal to 25.7 mm. Its cutoff frequency (TE_{11} mode) is 6.84 GHz and the next higher cutoff frequency (TM_{01} mode) is 8.94 GHz.

The impulse excitation is such that the TM_{01} mode does not propagate. A bandpass Gaussian pulse with Fourier spectrum symmetrical about $f_0 = 7.5$ GHz and a bandwidth about ± 0.5 GHz excites a z-directed dipole centered in the circular waveguide and $\lambda_g/4$ from the closed end. The 3-D grid resolution is $\lambda_0/40 = 1$ mm. The mesh for the boundary of the horn antenna has 2358 triangles and 3492 edges whose lengths are longer than $\lambda_0/20$ and shorter than $\lambda_0/5$.

Figs. 11 and 12 show the radiation pattern in the E-plane and in the H-plane at $f_0 = 7.5$ GHz. Good agreements are obtained.

IV. Conclusion

We have proposed a new fictitious domain method for the study of scattering by PEC. We introduced the surface electric current density defined on the interfaces between vacuum and PEC. A simple coupling law between the surface electric current density and the electric field ensures the vanishing of the tangential components of the electric field on the boundaries of the PEC.

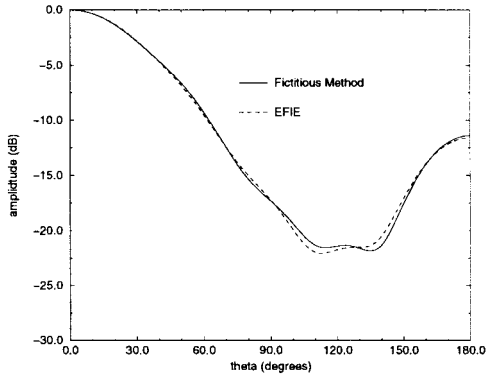

Fig. 12. Radiation pattern of the horn antenna in the H-plane, frequency $F = 7.5$ GHz. Comparison of the fictitious domain method and EFIE.

Then we use a regular 3-D cubic lattice for the electromagnetic field and triangular surface patching for the surface electric current density. We choose these two meshes so that the shortest edge of the triangular patches of the surface mesh is longer than the space increment h in order to obtain a small positive definite sparse system whose solution is the surface electric current density at each time step.

The remarkable property of the numerical scheme of the fictitious domain method is a simple stability criterion, which is independent of the triangular patching of the boundaries of the PEC. Numerical results show the efficiency of this method, particularly for sharp bodies and curved metallic bodies.

The numerical scheme of the fictitious domain method looks like Yee's scheme, but with a special treatment for the PEC. This allows us to use the usual techniques developed for FDTD like absorbing boundary conditions. For example it is possible to model PEC with the fictitious domain method and other materials like dielectric or lossy materials with a FDTD method.

Finally, future works will try to adapt the fictitious domain method to model dielectric materials, and thin wires.

Acknowledgment

The authors would like to thank F. Millot of CERFACS, Toulouse, France, for numerous stimulating discussions and J. Roberts of INRIA, Rocquencourt, France, for her help.

References

[1] K. S. Yee, "Numerical solution of initial boundary value problems involving Maxwell's equation in isotropic media," *IEEE Trans. Antennas Propagat.*, vol. AP-14, no. 3, pp. 302–307, 1966.
[2] R. Holland, "Pitfalls of staircase meshing," *IEEE Trans. Electromagn. Compat.*, vol. 35, pp. 434–439, 1993.
[3] D. Sheen, S. Ali, M. Abouzahra, and J. A. Kong, "Application of the three-dimensional finite-difference time-domain method to the analysis of planar microstrip circuits," *IEEE Trans. Microwave Theory Tech.*, vol. 38, pp. 849–856, 1990.
[4] J.-F. Lee, R. Palendech, and R. Mittra, "Modeling three-dimensional discontinuities in waveguides using nonorthogonal FDTD algorithm," *IEEE Trans. Microwave Theory Tech.*, vol. 40, pp. 346–352, 1992.
[5] T. G. Jurgens, A. Taflove, K. R. Umashankar, and T. G. Moore, "Finite-difference time-domain modeling of curved surfaces," *IEEE Trans. Antennas Propagat.*, vol. 35, pp. 1248–1257, 1987.

[6] T. G. Jurgens and A. Taflove, "Three-dimensional contour FD-TD modeling of scattering from single and multiple bodies," *IEEE Trans. Antennas Propagat.*, vol. 41, pp. 1703–1708, 1993.
[7] C. J. Railton and I. J. Craddock, "Stabilized CPFDTD algorithm for the analysis of 3-D PEC structures," in *Proc. Inst. Elect. Eng. Microwaves, Antennas, Propagat.*, vol. 143, no. 5, pp. 367–372, 1996.
[8] S. Dey and R. Mittra, "A locally conformal FDTD algorithm for modeling 3-D perfectly conducting objects," *IEEE Microwave Guided Wave Lett.*, vol. 7, pp. 273–275, 1997.
[9] J. Anderson, M. Okoniewski, and S. S. Stuchly, "Practical 3-D contour/staircase treatment metal in FDTD," *IEEE Microwave Guided Wave Lett.*, vol. 6, pp. 146–148, 1996.
[10] C. Atamian and P. Joly, "Une analyze de la méthode des domaines fictifs pour le problème de Helmholtz extérieur," *Math. Modeling*, vol. 27, no. 3, pp. 251–288, 1993.
[11] A. Bespalov, "Application of the fictitious domain method to the solution of the Helmholtz equation in the unbounded domain," Rocquencourt, Tech. Rep. INRIA, 1992.
[12] R. Glowinski, T. W. Pan, and J. Periaux, "A fictitious domain method for Dirichlet problem and applications," *Comput. Methods Appl. Mech. Eng.*, vol. 111, pp. 283–303, 1994.
[13] F. Collino, P. Joly, and F. Millot, "Fictitious domain method for unsteady problems: Application to electromagnetic scattering," in *3rd Int. Conf. Math. Numer. Aspects Wave Propagat.*, Mandelieu, France, June 1995.
[14] ——, "Fictitious domain method for unsteady problems: Application to electromagnetic scattering," *J. Comput. Phys.*, to be published.
[15] S. Garcés, "Application des méthodes de domaines fictifs à la modélization des structures rayonnantes tridimensionnelles," Ph.D. dissertation, École Nationale de l'Aéronautique et de l'Espace, Toulouse, France, Dec. 1997.
[16] G. C. Hsiao and R. E. Kleinman, "Mathematical foundations for error estimation in numerical solution of integral equations in electromagnetic," *IEEE Trans. Antennas Propagat.*, vol. 45, pp. 316–328, Mar. 1997.
[17] J. C. Nédélec, "Mixed finite elements in R^3," *SIAM J. Numer. Anal. Math. Modeling*, vol. 28, pp. 1610–1634, 1991.
[18] P. A. Raviart and J. M. Thomas, *Introduction à l'Analyze Numérique des Équations aux Dérivées Partielles*. Paris, France: Masson, 1992.
[19] A. Taflove, *Computational Electrodynamics—The Finite-Difference Time-Domain Method.* Norwood, MA: Artech House, 1995.
[20] V. Girault and R. Glowinski, "Error analysis of a fictitious domain method applied to a Dirichlet problem," *Japan J. Indust. Appl. Math.*, vol. 12, no. 3, pp. 487–514, 1995.
[21] J. P. Berenger, "A perfectly matched layer for the absorption of electromagnetic waves," *J. Comput. Phys.*, vol. 114, pp. 185–200, 1994.
[22] D. N. Buechler, D. H. Roper, C. H. Durney, and D. A. Christensen, "Modeling sources in the FD-TD formulation and their use in quantifying source and boundary condition errors," *IEEE Trans. Microwave Theory Tech.*, vol. 43, no. 4, pp. 810–914, 1995.
[23] W. E. Blore, "The radar cross section of ogives, double-backed cones, double-rounded cones, and cone spheres," *IEEE Trans. Antennas Propagat.*, pp. 582–590, 1964.
[24] C. A. Balanis, *Advanced Engineering Electromagnetics.* New York: Wiley, 1989.

Francis Collino was born in 1958. He received the Eng. degree from École Nationale Supérieure des Mines, Paris, France, in 1982, and the Ph.D. degree in applied mathematics from University Paris Dauphine, France, in 1987.

In 1983, he was with IFP French National Research Institute for oil. Since 1991 he has been with INRIA, Institut Nationale de Recherche en Informatique et Automatique, working on Project ONDES. His areas of interest include mathematical modeling and numerical analysis of wave propagation phenomena with applications to various areas of physics (acoustics, elasticity, and electromagnetism).

Sylvain Garcés received the Ph.D. degree from École Nationale Superieurs Aeronautique et Espace, Aeronautical and Space Grande École of Engineering, Toulouse, France, in 1993.

In 1994, he was with Cerfacs, Toulouse, France, and in 1996 he was with CNET, La Turbie, France, working on the fictitious domain method for electromagnetism. He then joined the SEMA group 1998 to work at the Flight Dynamics Center of CNES, Toulouse, France, on launching and early phase operations for geostationary satellites.

Patrick Joly was born in 1957. He received the Eng. degree from École Centrale de Paris, France, in 1980, the D.E.A in numerical analysis from University Pierre et Marie Curie, Paris, France, in 1981, and the Ph.D. (applied mathematics) and Doctorat d'Etat degree (applied mathematics), both from University Paris Dauphine, France, in 1983 and 1987, respectively.

He is currently Director of Research at INRIA (Institut National de Recherche en Informatique et Automatique) and leader of the Project ONDES. He is also Maitre de Conferences in Applied Mathematics at École Polytechnique. His specialties include mathematical modeling and the numerical analysis of wave propagation phenomena with applications to various areas of physics including acoustics, elasticity, electromagnetism, hydrodynamics, and fluid-structure interaction.

Dr. Joly was awarded the Blaise Pascal Prize from the French Academy of Sciences in 1994.